Nitrogen-Doped Graphene Nanoplatelets from Simple Solution Edge-Functionalization for n-Type Field-Effect Transistors

Dong Wook Chang,[†,⊥] Eun Kwang Lee,[‡,⊥] Eun Yeob Park,[‡] Hojeong Yu,[‡] Hyun-Jung Choi,[§] In-Yup Jeon,[§] Gyung-Joo Sohn,[§] Dongbin Shin,[§] Noejung Park,[§] Joon Hak Oh,*[‡] Liming Dai,*[∥] and Jong-Beom Baek*[§]

[†]Department of Chemical Systematic Engineering, Catholic University of Daegu, 100, Hayang, 712-702, South Korea

[‡]School of Nano-Bioscience and Chemical Engineering, KIER-UNIST Advanced Center for Energy, Low-Dimensional Carbon Materials Center, Ulsan National Institute of Science and Technology (UNIST), Ulsan 689-798, South Korea

[§]Interdisciplinary School of Green Energy, Low-Dimensional Carbon Materials Center, Ulsan National Institute of Science and Technology (UNIST), Ulsan 689-798, South Korea

[∥]Department of Macromolecular Science and Engineering, Case Western Reserve University, Cleveland, Ohio 44106, United States

Ⓢ *Supporting Information*

ABSTRACT: The development of a versatile method for nitrogen-doping of graphitic structure is an important challenge for many applications, such as energy conversions and storages and electronic devices. Here, we report a simple but efficient method for preparing nitrogen-doped graphene nanoplatelets *via* wet-chemical reactions. The reaction between monoketone (C=O) in graphene oxide (GO) and mono-amine-containing compound produces imine (Shiff base) functionalized GO (iGO). The reaction between α-diketone in GO and 1,2-diamine (*ortho*-diamine)-containing compound

gives stable pyrazine ring functionalized GO (pGO). Subsequent heat-treatments of iGO and pGO result in high-quality, nitrogen-doped graphene nanoplatelets to be designated as hiGO and hpGO, respectively. Of particular interest, hpGO was found to display the n-type field-effect transistor behavior with a charge neutral point (Dirac point) located at around −16 V. Furthermore, hpGO showed hole and electron mobilities as high as 11.5 and 12.4 $cm^2V^{-1}s^{-1}$, respectively.
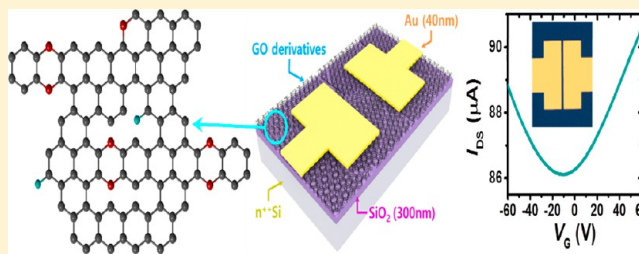
INTRODUCTION

Graphene, composed of carbon atoms densely packed into a 2D honeycomb crystal lattice, has attracted tremendous interest for various applications due to its fascinating properties, such as a large surface area, high thermal/electrical conductivity, and high mechanical strength.[1−3] Several methods, including mechanical exfoliation,[1] epitaxial growth,[4] structural restoration from graphene oxide (GO),[3] and bottom-up synthesis from small organic molecules,[5] have been developed to prepare various graphene structures. Among them, graphitization of GO has been most widely investigated due to its good processability and capability of mass production.[6,7]

On the other hand, it is known that graphene is a zero band gap semiconductor with a carrier mobility as high as 2×10^5 $cm^2V^{-1}s^{-1}$, which is an order of magnitude higher than that of silicon wafer.[8] Therefore, the modulation of their electrical properties (e.g., the band gap opening and tuning) is of great importance to performance optimization for the graphene-based optoelectronic devices.[9−13] One of the most feasible approaches to control the electronic properties of graphene is chemical doping by incorporation of heteroatoms (e.g., boron, nitrogen) into graphitic framework, which can not only alter the band structure but also generate specific charge carriers

(holes and electrons).[10,13,14] In particular, nitrogen-doped graphene has attracted great attention due to its superior performance in various devices, including fuel cells,[15−18] batteries,[19] and field-effect transistors (FETs).[10,12,13,20,21]

In general, graphene-based FETs show p-type behaviors due to the adsorption of oxygen or water in air.[10] Therefore, it is more challenging to develop n-type graphene compared with the easily obtainable p-type graphene. Hitherto, several methods, including chemical vapor deposition (CVD),[12,22] annealing with NH_3 after N^+ ion irradiation of mechanically exfoliated graphene,[13] supercritical reaction,[20] and post-treatment of GO,[21,23] have been developed to produce nitrogen-doped graphene, which shows unique n-type behaviors in FETs. Although nitrogen-doped graphene prepared from GO is desirable for mass production with good reproducibility, it shows relatively poorer performances in FETs than its counterparts from other synthetic methods due to a relatively low nitrogen doping level and an inefficient structural restoration intrinsically associated with the reduced GO.[21,23]
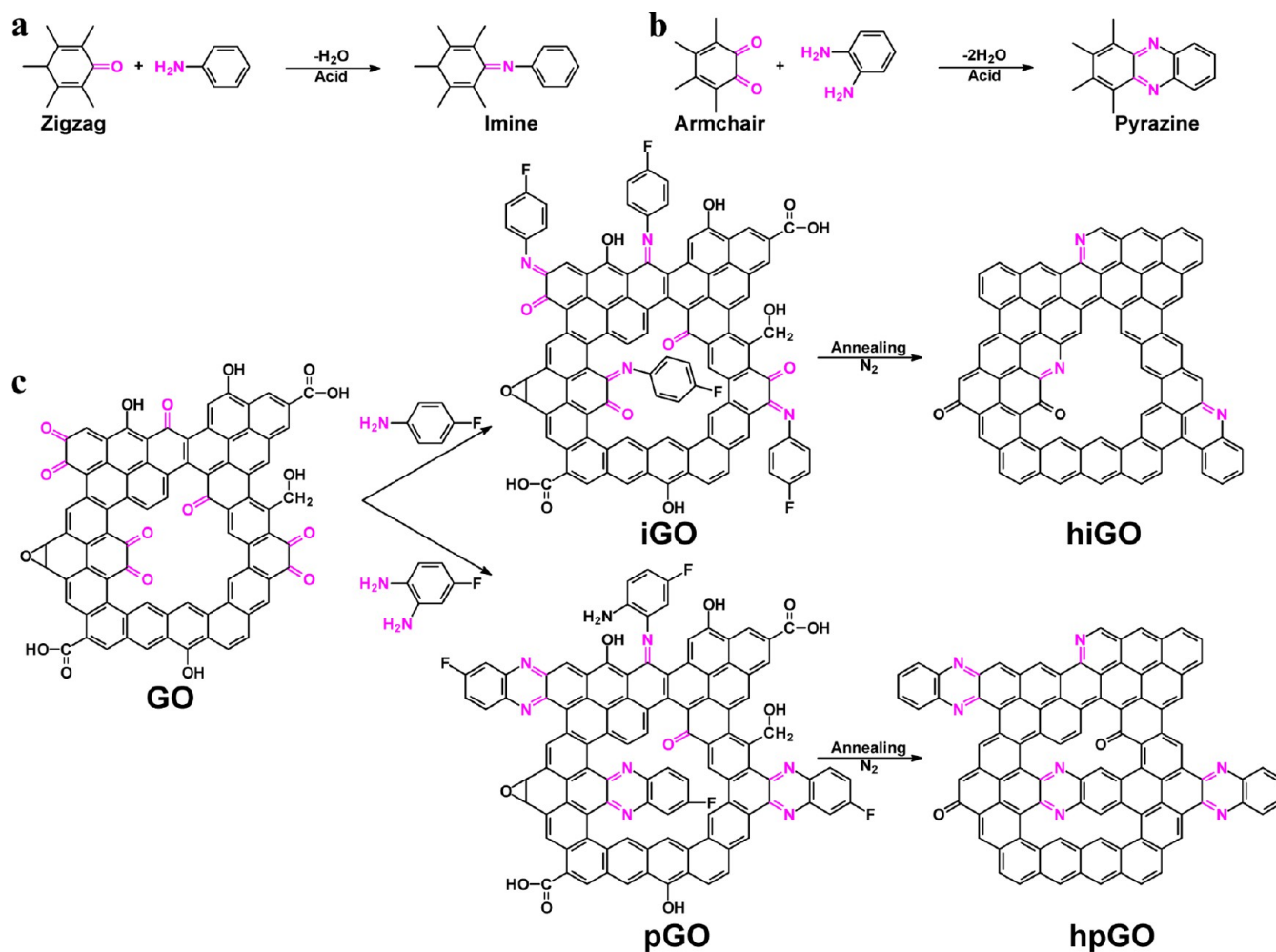
Figure 1. Schematic representations: (a) the formation of imine (Schiff base) from the condensation reaction between monoketone (C=O) and aniline (monoamine); (b) the formation of aromatic pyrazine rings from the double-condensation reaction between α-diketone and 1,2-diaminobenzene (*ortho*-diamine); (c) the reaction between GO and 4-fluoroaniline or 1,2-diamino-4-fluorobenzene to yield iGO or pGO, respectively. Subsequent heat treatment of iGO and pGO under nitrogen atmosphere produced hiGO and hpGO, respectively.

Recently, we developed a facile and scalable synthetic method to produce nitrogen-doped graphene nanoplatelets and their large-area high-quality films using Friedel−Crafts acylation reaction between the pristine graphite and 4-aminobenzoic acid.[16] Although outstanding electrocatalytic activity for oxygen reduction reaction (ORR) was obtained, they showed a relatively low nitrogen-doping level of around 1.63 wt % after heat treatment. On the other hand, several nitrogen-doped graphene nanoplatelets with high nitrogen-doping levels have been prepared by hydrothermal reaction[24−27] and wet-chemical reactions between GO and nitrogen-containing small molecules.[28] However, they showed relatively poorer device performances, probably due to the larger structural defects originated from less controlled reaction mechanisms and existing oxygenated groups in graphitic structure. In order to enhance the performance of graphene-based devices (e.g., FETs and fuel cells), therefore, the development of facile and controlled preparation methods for post-treatment of GO to produce nitrogen-doped graphene nanoplatelets with high doping levels and lower structural defects is highly desirable.

Herein, we, for the first time, report a highly efficient synthetic protocol for producing nitrogen-doped graphene *via* simple acid-catalyzed dehydration reactions between aromatic ketone (C=O) and primary amine (NH$_2$) groups. Figure 1a shows the condensation reaction between the monoketone (C=O) in GO and single amine to form imine (−C=N−, Schiff base) linkage. The double-condensation reaction between α-diketone (O=C−C=O) and 1,2-diamine (or *ortho*-diamine) produces stable aromatic pyrazine rings (Figure 1b). In GO, the single ketone is most likely observed at zigzag edges, while the α-diketone should exclusively exist at armchair edges. Since the driving force for the reaction between α-diketone and *ortho*-diamine is aromatization, the formation of aromatic pyrazine rings is expected to be much more favorable than the imine formation. Indeed, density functional theory (DFT) calculations revealed that the formation energies of imine and pyrazine are +11.9 and −20.4 kcal/mol, respectively (Figure S1). On this basis, two types of aromatic amine compounds containing fluorine atoms were used as an indicator (e.g., 4-fluoroaniline, 1,2-diamino-4-fluorobenzene), for example, for X-ray photoelectron spectroscopic (XPS) measurements, to react with GO (Figure 1c) to yield nitrogen-containing GO in the forms of imine (iGO) and pyrazine (pGO) (experimental details are described in Supporting Information, SI). Imine linkage is known to be less stable against hydrolysis and thermolysis than aromatic pyrazine rings. As shown in Figure 1c, the subsequent heat treatment (900 °C
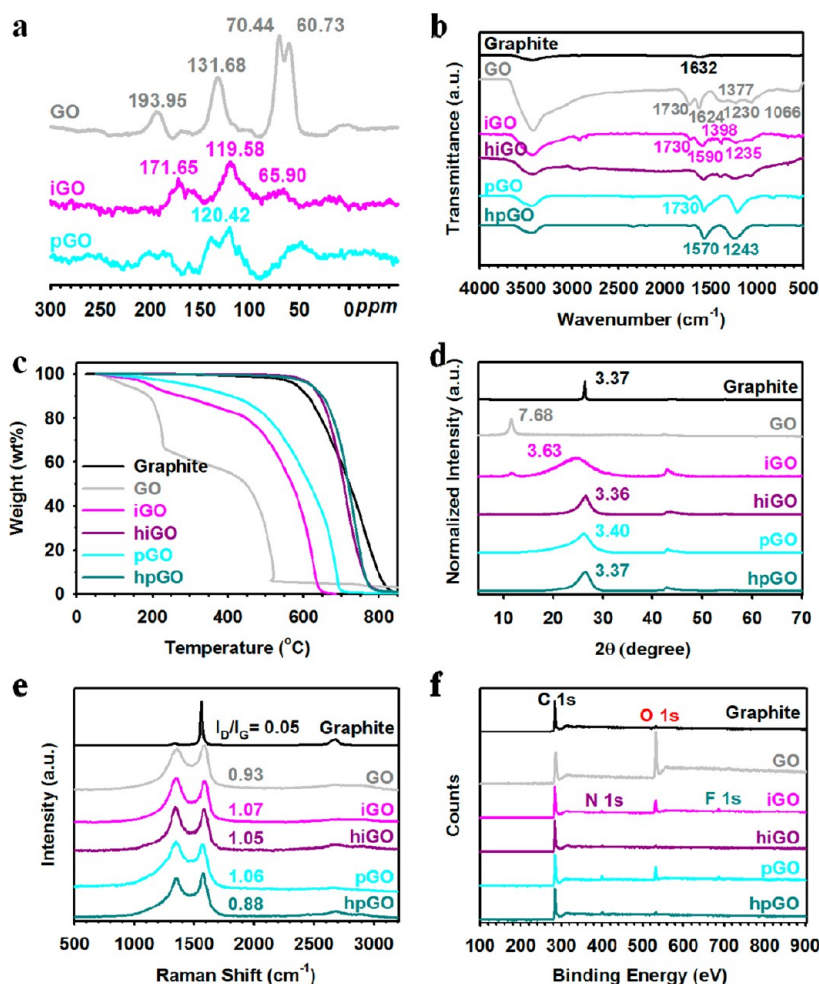
Figure 2. (a) Solid-state ^{13}C MAS NMR spectra of GO, iGO, and pGO; (b) FT-IR spectra; (c) TGA thermograms obtained with a heating rate of 10 °C min^{-1}; (d) XRD diffraction patterns. The numbers are *d*-spacings in Å; (e) Raman spectra; (f) XPS survey spectra of graphite, GO, iGO, pGO, hiGO, and hpGO.

for 2h) of iGO and pGO under nitrogen atmosphere produced heat-treated iGO (hiGO) and pGO (hpGO), respectively. Chemical reduction process (e.g., using hydrazine) was not applied to our system, since it can cause an additional doping effect on the GO plate.[29−31] FETs fabricated from hiGO and hpGO exhibited high hole and electron mobilities of up to 11.5 and 12.4 cm^{2}V^{-1}s^{-1}, respectively. The Dirac point was negatively shifted to −16 V, indicating the successful n-type doping. Our doping method allowed for a high-quality and efficient nitrogen-doping of graphene, and thus it will pave a viable way toward the tuning of electronic properties of graphene.

■ RESULTS AND DISCUSSION

The chemical compositions of all samples (e.g., graphite, GO, iGO, hiGO, pGO, and hpGO) were characterized by elemental analyses (EA), and the results are summarized in Table S1. The starting graphite is mostly composed of carbon atom (98.81 wt %), while GO contains high oxygen content (45.45 wt %). However, iGO and pGO have dramatically decreased oxygen contents of 19.41 and 9.85 wt %, respectively, while the corresponding nitrogen contents have increased to 2.75 and 9.05 wt %. It is noteworthy that pGO has a more significant compositional change than iGO, supporting that the formation of pyrazine ring is much more favorable than the imine

formation. As a result, the ratio of nitrogen (N)/carbon (C) is about 1/9.55, which is, so far, the highest nitrogen content among all nitrogen-doped graphene materials produced by solution processes.[16,24,28] Hence, the scalable production of nitrogen-doped graphene nanoplatelets with such a high nitrogen content should be one of the notable achievements for many applications. Although similar nitrogen-doping levels have been obtained through CVD[10,19] and heat treatment of GO with nitrogen-containing molecules,[15,21,32,33] the former has a significant drawback due to the scalability, and the latter often shows a poor quality for the resultant nitrogen-doped graphene for device applications.[10,21,33] However, the formation of stable pyrazine rings between α-diketone functionalities at the armchair edges of GO and *ortho*-diamine derivatives can spontaneously take place during acid catalyzed dehydration reactions, because of the large thermodynamic gain by aromatization (−20.4 kcal/mol). Further heat-treatment of iGO and pGO at elevated temperature under nitrogen atmosphere not only removed remnant oxygenated groups but also restored graphitic structure (Figure 1c). The resultant heat-treated samples (i.e., hiGO and hpGO) showed the ratios of oxygen (O)/C approaching to zero (Table S1), which is the lowest value ever reported so far.[34] Furthermore, hiGO and hpGO have maintained high nitrogen contents of 3.12 and

7.73%, respectively (Table S1). Note that the higher N/C ratio of hpGO indicates high thermal stability of pyrazine ring.

The solid state ^{13}C magic-angle spinning (MAS) NMR spectra of GO, iGO, and pGO indicate significant structural changes have been induced by the acid-catalyzed reactions between GO and amine-containing molecules (Figure 2a). The NMR spectrum of GO shows that the peaks at 60.73 and 70.44 ppm correspond to ^{13}C nuclei near epoxide and hydroxyl groups, respectively.[7,35] The resonance peak at 131.68 ppm is assignable to unoxidized sp^2 carbons in graphitic structure. The peak at 193.95 ppm presumably attributes to carbonyl carbons.[7,35] However, the peak intensities of oxygenated (60.73 and 70.44 ppm) and carbonyl (193.95 ppm) carbons have been greatly reduced for the spectra of iGO and pGO in respect to the graphitic sp^2 carbon peak, which also shifted from 131.68 ppm to around 120 ppm. After conversion of ketone (C=O) groups by acid-catalyzed imine (C=N) formation (see Figure 1), the carbonyl peak around 193.95 ppm was shifted to 171.65 ppm for iGO.[35] Interestingly, pGO displays major sp^2 carbon peak near 120.42 ppm with traces of minor peaks around 48.43 and 186.48 ppm corresponding to ^{13}C nuclei near epoxide and carbonyl groups, respectively. Furthermore, the sharp decrease of ^{13}C nuclei near hydroxyl groups at 70.44 ppm was observed due to the acid-catalyzed dehydration reactions at high temperature between hydroxyl groups and adjacent hydrogen atoms.[36−38] These results indicate that graphitic structure has already been significantly restored by the formation of aromatic pyrazine rings at the edges (Figure 1c) as well as the transformation of sp^3 C−C bonds into sp^2 C−C bonds. Like heat-treated GO,[34] the formation of aromatic pyrazine rings in pGO and subsequent heat treatment could also promote spontaneous reduction of GO at the same time.

FT-IR spectroscopic measurements using KBr pellets were also conducted to further understand the structural changes before and after reactions and subsequent heat treatments. As shown in Figure 2b, the pristine graphite shows only a weak characteristic band of the vibration mode of adsorbed water molecules at 1632 cm^{-1}.[39] The spectrum from GO displays several oxygenated bands at 1730 ($\nu_{C=O}$), 1624 ($\nu_{C=C}$), 1377 (ν_{O-H}), 1230 ($\nu_{phenolic}$), and 1066 cm^{-1} (ν_{C-O}), along with hydroxyl bands (3400 cm^{-1}), and it agrees well with literatures.[10,35,40] However, iGO and pGO show the two characteristic peaks, in-plane vibrations of aromatic C=C sp^2 hybridized carbon in graphitic network[41,42] at around 1590 cm^{-1} and notable C=N stretching mode[43] near 1240 cm^{-1}, in conjunction with a concomitant decrease of oxygenated peaks including carbonyl peak at 1730 cm^{-1}. In addition, both characteristic peaks of ν_{O-H} (1377 cm^{-1}) and ν_{C-O} (1066 cm^{-1}) disappeared due to the acid-catalyzed dehydration reaction between hydroxyl groups and adjacent hydrogen atoms in GO. Furthermore, the complete removal of carbonyl group was obtained after post-annealing process at an elevated temperature in hiGO and hpGO. These spectroscopic results are in accordance with the structures proposed in Figure 1c.

Thermogravimetric analysis (TGA) of all samples was conducted in air, and the results are presented in Figure 2c. As expected, GO shows a weight loss starting from around 100 °C, which is attributed to the elimination of bound water between layers and hygroscopic functional groups. The catastrophic weight loss near 200 °C is related to the loss of oxygenated functional groups before the complete oxidative decomposition of the graphitic substrate over 200−500 °C. On

the other hand, the acid-catalyzed reactions have induced a significant reduction and elimination of edge-functionalized groups via the formation of iGO and pGO, which display much improved thermal stability. Furthermore, heat-treated samples, hiGO and hpGO, show the highest thermal stability, compared favorable or even better than the pristine graphite. The great enhancement in thermal stability is presumably due to the high degree of structural restoration in hiGO and hpGO.

The powder X-ray diffraction (XRD) patterns of all samples are shown in Figure 2d. The pristine graphite shows a sharp strong peak at $2\theta = 26.4°$ (d-spacing ~ 3.37 Å), while GO displays a broad weak peak at ca.11.7° (d-spacing ~ 7.68 Å). The increase in d-spacing of GO is due to a lattice expansion by oxygenated functional groups and bound small molecules between layers. However, the broad peak for iGO is significantly shifted to 24.4° (d-spacing ~ 3.63 Å), and the sharper and narrower peak for hiGO is further shifted to 26.5° (d-spacing ~ 3.36 Å). The peak location (d-spacing) is almost the same as that of the pristine graphite (d-spacing ~ 3.36 Å). Interestingly, compared with iGO, pGO shows relatively much narrower peak at 26.1° (d-spacing ~ 3.40 Å), which is already comparable to that of the pristine graphite, indicating that spontaneous reduction and the formation of aromatic pyrazine rings have occurred. After heat treatment, the peak from hpGO was slightly shifted to 26.4° (d-spacing ~ 3.37 Å). These results, once again, indicate that the acid-catalyzed reactions and post-heat treatments are feasible approaches for the preparation of well-ordered graphene nanoplatelets with high nitrogen contents.

Raman spectra obtained from the powder samples are shown in Figure 2e. The pristine graphite shows the G and 2D bands at 1564 and 2679 cm^{-1}, respectively. Due to the large grain size, its D band at 1335 cm^{-1} associated with the edge distortion is negligible, and thus the ratio of the D to G-band intensities (I_D/I_G) is ~0.05. In contrast, GO showed a broad and strong D band at 1355 cm^{-1} with a high I_D/I_G ratio of 0.93, indicating the reduction in size of the in-plane sp^2 domains and increase in structural distortions. Furthermore, the G band at 1588 cm^{-1} was slightly up-shifted with respect to that of graphite (1564 cm^{-1}) due to the presence of isolated double bonds, which shows the higher resonance frequencies than that of G band in graphite.[44] iGO also showed similar D and G bands at 1347 and 1563 cm^{-1}, respectively, but it has a higher I_D/I_G ratio of 1.07 than that of GO ($I_D/I_G = 0.93$), indicating the presence of large amounts of topological defects during acid-catalyzed nitrogen-doping process.[12] After heat treatment, hiGO shows D and G bands at 1347 and 1576 cm^{-1}, respectively, with a similar I_D/I_G ratio (1.05) to iGO (1.07). Interestingly, the significant decrease in I_D/I_G ratio of hpGO (0.88) from pGO (1.06) was observed, which can be also closely related to the efficient structural restoration of graphitic framework during the postannealing process to yield high-quality hpGO.

The chemical composition changes during the acid-catalyzed reactions and post-annealing process were further monitored by XPS (Figure 2f). The N 1s and F 1s peaks in iGO and pGO were clearly detected at around 400 and 687 eV, respectively, to ensure incorporation of nitrogen and fluorine. After heat treatment at 900 °C, both N 1s and F 1s peaks in hiGO largely disappeared, while hpGO still maintained the N 1s peak without F 1s peak. These results indicated that the aromatic pyrazine ring is thermally stable compared with imine and C-fluorine linkages (see Figure 1). As shown in Figure S2, the high-resolution C 1s peak from GO can be deconvoluted into
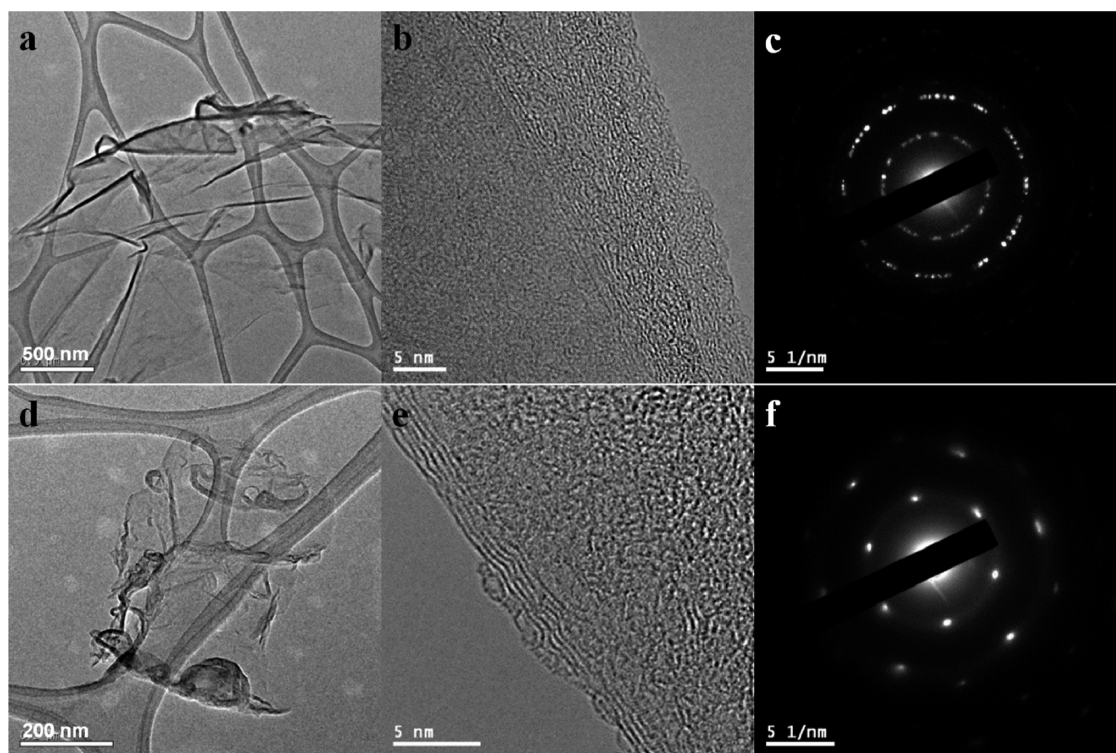
Figure 3. (a, b) TEM images of pGO at different magnifications and (c) corresponding SAED pattern taken at the relatively flat area. (d, e) TEM images of hpGO at different magnifications and (f) corresponding SAED pattern.

several peaks corresponding to the sp^2 carbon at 284.8 eV and other oxygenated carbons, such as C−O, C=O, and O−C=O, respectively (Figure S2b).[7,34,37] Although the high-resolution C 1s spectra of iGO (Figure S2c) and pGO (Figure S2e) also show minor peaks higher than 284.8 eV, their intensities are much lower compared with those of GO. Furthermore, a new peak at 285.8 eV, which is reflecting a different bonding nature of carbon (e.g., C=N[12]), was observed in iGO and pGO. After heat-treatment, the C 1s spectra of hiGO and hpGO became similar to that of the pristine graphite with a major peak at 284.4 eV and a minor peak at 285.8 eV, corresponding to sp^2 carbon and C=N, respectively. As shown in Figure S3, the high-resolution N 1s spectra also show the significant compositional changes after acid-catalyzed nitrogen-doping reactions for iGO and pGO and subsequent heat treatments for hiGO and hpGO. While the pristine graphite and GO have no detectable nitrogen peaks (Figure S3a and S3b), iGO exhibits a prominent N 1s peak at 399.7 eV, which is attributable to imine-N (C=N).[45] Interestingly, pGO displays three peaks at 398.5, 399.7, and 400.5 eV, corresponding to pyrazine-N,[46] imine-N, and amine-N,[45] respectively. Although characteristic peaks of imine (−C=N−) and amine (−NH$_2$) bonds, from the reaction between monoketone in GO and *ortho*-diamine, are still observed in pGO, the existence of nitrogen in different environment like pyrazine was also confirmed by XPS analysis. Upon the post-annealing, the graphitic nitrogen peak at 400.7 eV for hiGO and hpGO was greatly enhanced, which is accompanied by the appearance of an additional peak at around 397.9 eV attributable to pyridinic-N and its resonance form in graphitic structure (Figure 1c).[3,16,47] Therefore, it can be deduced that the characteristic nature of nitrogen atoms was changed before and after the heat treatment. In addition to carbon and nitrogen atoms, the F atom in 4-fluoroaniline and 1,2-diamino-4-

fluorobenzene moieties of iGO and pGO can serve as an XPS probe for elucidating the structural changes during the post-annealing. As expected, Figure S4a and S4b shows no F 1s peak for the pristine graphite and GO, whereas a strong F 1s peak was observed at around 686.8 eV for both iGO and pGO. For hiGO and hpGO, however, the F 1s peak completely disappeared (Figure S4d and S4f), indicating that all fluorine atoms were stripped off from the iGO and pGO by the heat treatment.[48] The above spectroscopic and diffraction measurements are, therefore, consistent well with the structural changes during the acid-catalyzed reactions and subsequent heat treatment to produce nitrogen-doped graphene, as proposed in Figure 1c.

Comparing with GO, the iGO and pGO displayed a significantly enhanced flat UV−vis absorbance up to 900 nm (Figure S5), indicating that the electronic conjugation within the graphitic structure was largely retained during the acid-catalyzed reactions.[34] The flat absorbance was further enhanced for the heat-treated hiGO and hpGO due to the effective structural restoration of graphitic framework during the subsequent heat-treatments.

The morphological and microstructural changes were investigated by scanning electron microscopy (SEM) and transmission electron microscopy (TEM). As can be seen in Figure S6, GO appears to be thin and densely packed sheets (Figure S6a), whereas those of iGO (Figure S6b), pGO (Figure S6c), hiGO (Figure S6d), and hpGO (Figure S6e) demonstrated wrinkled paper-like structures with relatively high-electron transparency. TEM images obtained from the pGO and hpGO at low magnification also exhibit wrinkled paper-like morphology (Figure 3a and 3d). The edge-on views at a high magnification show highly crystalline interior (Figure 3b and 3e), indicating a high degree of structural restoration had occurred during the acid-catalyzed reactions and subsequent
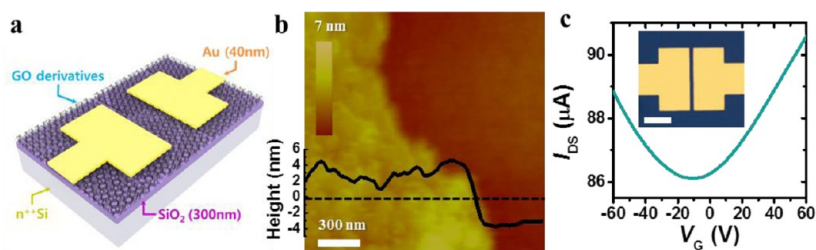
Figure 4. (a) Schematic illustration of FETs using GO derivatives as the active layers; (b) a tapping-mode AFM image of hpGO film on a SiO_2/Si wafer. The embedded graph is the thickness profile along the dashed line; (c) the typical transfer curve of hpGO FET at $V_D = 1$ V. The inset is an optical image of hpGO FET with photolithographically patterned gold electrodes ($W/L = 40$, $L = 3$ μm). Scale bar is 40 μm.

heat treatments. The corresponding selected area electron diffraction (SAED) patterns further support the high crystallinity of pGO and hpGO (Figure 3c and 3f). The SAED pattern of pGO given in Figure 3c shows ring-like diffraction spots, which indicates the regional disruption of crystal lattice in pGO. After the heat treatment, however, hpGO shows a symmetric hexagonal diffraction pattern, which is ascribed to a typical diffraction pattern of graphite,[49,50] suggesting that graphitic structure had been well-restored in hpGO.

To shed light on the electrical properties of the nitrogen-doped graphene nanoplatelets, we fabricated FETs using the GO derivatives as the active layers. The schematic illustration of a typical FET device is presented in Figure 4a, while the details on the film preparation are described in the SI. Atomic force microscope (AFM) analysis on the hpGO film revealed that the average (mean) thickness of the sample (out of 19 samples) was 4.5 $\pm$ 0.6 nm (Figure 4b), which corresponds to the stacking of 3 to 5 layers of hpGO sheets. The films of other GO derivatives also exhibited a similar thickness of 4−5 nm. The inset of Figure 4c displays the optical image of representative hpGO FET placed on a SiO_2/Si wafer with photolitho-graphically patterned gold electrodes (the channel width-to-length ratio (W/L) = 40, $L = 3$ μm). Figure 4c exhibits a typical transfer curve of the hpGO FETs. The hole and electron mobilities were extracted from the linear regime of the transfer characteristics using the following equation:

$$I_D = \mu \frac{W}{L} C_i V_D (V_G - V_{th})$$

where I_D is drain current, μ is field-effect mobility, C_i is the specific capacitance of the dielectric, V_D is drain voltage, V_G is gate voltage, V_{th} is threshold voltage, and W and L are channel width and length, respectively. Calculated hole and electron mobilities from the transfer curve in Figure 4c were 9.0 and 7.9 $cm^2V^{-1}s^{-1}$, respectively. Dirac point, in which charges are neutralized, was found to be −10 V, indicating that nitrogen doping was performed successfully. The small on/off current ratio indicates the band gap of hpGO was not opened. The artificial and regular lattice defects limit electron/hole mobilities and introduce a significant bandgap into monolayer graphene crystal.[51−53] The electrical performances of all the samples (i.e., GO, heat-treated GO (hGO), iGO, hiGO, pGO, and hpGO) were statistically compared by characterizing the $I-V$ characteristics of 64 FET devices for each sample, and the results are summarized in Table S2. As can be seen, the pristine GO did not show any field-effect behavior because of its insulating nature, whereas hGO exhibited hole and electron mobilities of 8.5 $\pm$ 0.4 and 6.3 $\pm$ 0.9 $cm^2V^{-1}s^{-1}$, respectively. The Dirac point was 28 $\pm$ 1.0 V, which clearly indicates a p-

doped nature by ambient adsorbates.[10,54,55] In contrast, iGO and pGO could exhibit field-effect characteristics without heat treatment because of the reduced content of oxygen induced by the dehydration reactions to form imines and aromatic pyrazine rings (see Figure 1c). The hiGO FETs exhibited hole and electron mobilities of 1.1 $\pm$ 0.02 and 0.5 $\pm$ 0.03 $cm^2V^{-1}s^{-1}$, respectively. The hpGO FETs showed hole and electron mobilities of 8.4 $\pm$ 0.9 and 7.1 $\pm$ 1.1 $cm^2V^{-1}s^{-1}$, respectively. The hpGO FETs have resulted higher mobilities and n-doping effect than those of hiGO FETs due to the higher nitrogen content and more structural restoration. The negative shift of the Dirac point in both hiGO and hpGO FETs clearly indicates that nitrogen doping on graphene nanoplatelets was success-fully performed.

In order to elucidate more intrinsic electrical properties of hpGO by minimizing the grain boundary effects, we fabricated hpGO FETs with a short channel length of 500 nm using e-beam lithography. The optical and AFM images of the top-contact FETs are displayed in Figure 5a and the inset of Figure
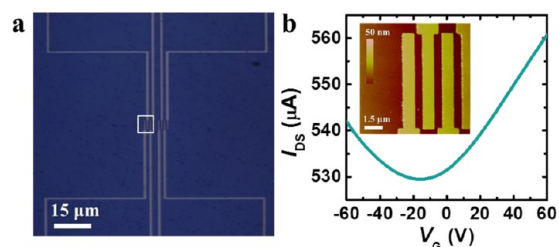

Figure 5. (a) Optical image of hpGO FETs with gold electrodes patterned using e-beam lithography ($W/L = 10$, $L = 500$ nm); and (b) the typical transfer curve obtained at $V_D = 0.5$ V. Inset is AFM image of the active channel area squared in (a).

5b. The typical transfer curve is presented in Figure 5b, where the maximum hole and electron mobilities were as high as 11.5 and 12.4 $cm^2V^{-1}s^{-1}$, respectively, with the Dirac point of −16 V. The average (mean) hole and electron mobilities obtained from 8 devices were 11.0 $\pm$ 0.5 and 12.2 $\pm$ 0.3 $cm^2V^{-1}s^{-1}$, respectively, with the Dirac point of −15 $\pm$ 1.2 V. The discrepancy in the mobility of the FETs patterning with gold electrodes by photolithography and e-beam lithography could be attributed to the difference in the channel length, which is closely related to the charge scattering induced by the grain boundaries. Short channel devices tend to hold less grain boundaries in the active channel, leading to the enhanced charge transport,[49,56] which was also confirmed by our supplementary experiments using a long channel length of 50 μm by thermally depositing the gold electrodes through the shadow mask (Figure S7). The difference in the Dirac point

values of the FETs prepared from photolithography and e-beam lithography might originate from the different process conditions that can produce different trap densities. In addition, the Dirac point shift and the device hysteresis were also tested by applying gate voltages with different sweep ranges in N_2 atmosphere. The hpGO FETs showed a little hysteresis (Figure S8 and Table S3). In the forward sweep (from negative to positive gate voltage), Dirac point was shifted to a more negative value, compared with the reverse sweep. The hysteresis is presumably due to the small portion of remaining oxygen-containing groups in hpGO that may act as charge trapping sites in the active channel. The hpGO FETs were also measured in ambient atmosphere (Figure S9 and Table S4). The Dirac point was still negative in ambient condition, indicating that n-type doping of hpGO was successfully performed.

CONCLUSIONS

We have developed a simple but efficient and reliable nitrogen-doping method *via* the reaction between the most commonly studied GO and primary amine-containing molecules in a solution phase. This newly developed doping method offers a powerful means to produce high-quality nitrogen-doped graphene nanoplatelets with the charge neutral point (Dirac point) located at around −16 V. Furthermore, the graphene nanoplatelets have hole and electron mobilities as high as 11.5 and 12.4 $cm^2V^{-1}s^{-1}$, respectively, in the short channel length (500 nm). The process developed in this study provides a simple solution method for large-scale production of high-quality nitrogen-doped graphene nanoplatelets for n-type FETs and new insights into the utilization of functional groups at the edges of GO to tune the electronic properties of graphene nanoplatelets.

EXPERIMENTAL SECTION

Materials and Preparation of Nitrogen-Doped Graphene. Graphite nanopowders (450 nm APS, 99.9% purity) from Nano-structured and Amorphous Materials, Inc. were used in this study. GO was prepared by the modified Hummers' method using the graphite nanopowders.[57] For the preparation of iGO, GO (1 g) was dispersed in an acetic acid (140 mL)/toluene (30 mL) mixture and applied sonication for 1 h. Then, 4-fluoroaniline (1 g) was added in the reaction mixture, which was heated under reflux with stirring overnight. Water formed during the dehydration reaction was completely removed by using Dean−Stark trap. After cooling down to room temperature, the mixture was filtered using a PTFE membrane (0.45 μm) and washed with plenty of THF and methanol. The product was further purified by Soxhlet extraction with methanol and THF. Finally, iGO was obtained as a black powder after drying under reduced pressure (0.05 mmHg) at 50 °C overnight. For the preparation of pGO, 1,2-diamino-4-fluorobenzene (1 g) was added in the same amount GO-containing solution and carried out using similar reaction and workup procedures for iGO. The heat treatment of iGO and pGO to produce hiGO and hpGO was conducted at 900 °C under nitrogen atmosphere for 2 h.

ASSOCIATED CONTENT

Ⓢ Supporting Information

Detailed FET device fabrications, DFT calculations and characterization data from EA, XPS, UV−vis spectra, SEM, and FET data. This material is available free of charge via the Internet at http://pubs.acs.org.

AUTHOR INFORMATION

Corresponding Author
jbbaek@unist.ac.kr; joonhoh@unist.ac.kr; liming.dai@case.edu
Author Contributions
⊥These authors contributed equally.
Notes
The authors declare no competing financial interest.

ACKNOWLEDGMENTS

REFERENCES

(1) Novoselov, K.; Geim, A.; Morozov, S.; Jiang, D.; Zhang, Y.; Dubonos, S.; Grigorieva, I.; Firsov, A. *Science* **2004**, *306*, 666.
(2) Eda, G.; Fanchini, G.; Chhowalla, M. *Nat. Nanotechnol.* **2008**, *3*, 270.
(3) Sun, Z.; James, D. K.; Tour, J. M. *J. Phys. Chem. Lett.* **2011**, *2*, 2425.
(4) Hass, J.; De Heer, W.; Conrad, E. *J. Phys.: Condens. Matter* **2008**, *20*, 323202.
(5) Kim, K. S.; Zhao, Y.; Jang, H.; Lee, S. Y.; Kim, J. M.; Kim, K. S.; Ahn, J.-H.; Kim, P.; Choi, J.-Y.; Hong, B. H. *Nature* **2009**, *457*, 706.
(6) Dreyer, D. R.; Park, S.; Bielawski, C. W.; Ruoff, R. S. *Chem. Soc. Rev.* **2010**, *39*, 228.
(7) Stankovich, S.; Dikin, D. A.; Piner, R. D.; Kohlhaas, K. A.; Kleinhammes, A.; Jia, Y.; Wu, Y.; Nguyen, S. T.; Ruoff, R. S. *Carbon* **2007**, *45*, 1558.
(8) Du, X.; Skachko, I.; Barker, A.; Andrei, E. Y. *Nat. Nanotechnol.* **2008**, *3*, 491.
(9) Martins, T.; Miwa, R.; da Silva, A. J.; Fazzio, A. *Phys. Rev. Lett.* **2007**, *98*, 196803.
(10) Wang, X.; Li, X.; Zhang, L.; Yoon, Y.; Weber, P. K.; Wang, H.; Guo, J.; Dai, H. *Science* **2009**, *324*, 768.
(11) Wehling, T.; Novoselov, K.; Morozov, S.; Vdovin, E.; Katsnelson, M.; Geim, A.; Lichtenstein, A. *Nano Lett.* **2008**, *8*, 173.
(12) Wei, D.; Liu, Y.; Wang, Y.; Zhang, H.; Huang, L.; Yu, G. *Nano Lett.* **2009**, *9*, 1752.
(13) Guo, B.; Liu, Q.; Chen, E.; Zhu, H.; Fang, L.; Gong, J. R. *Nano Lett.* **2010**, *10*, 4975.
(14) Wang, H.; Maiyalagan, T.; Wang, X. *ACS Catal.* **2012**, *2*, 781.
(15) Sheng, Z.-H.; Shao, L.; Chen, J.-J.; Bao, W.-J.; Wang, F.-B.; Xia, X.-H. *ACS Nano* **2011**, *5*, 4350.
(16) Jeon, I.-Y.; Yu, D.; Bae, S.-Y.; Choi, H.-J.; Chang, D. W.; Dai, L.; Baek, J.-B. *Chem. Mater.* **2011**, *23*, 3987.
(17) Qu, L.; Liu, Y.; Baek, J.-B.; Dai, L. *ACS Nano* **2010**, *4*, 1321.
(18) Wang, S.; Yu, D.; Dai, L.; Chang, D. W.; Baek, J.-B. *ACS Nano* **2011**, *5*, 6202.
(19) Reddy, A. L. M.; Srivastava, A.; Gowda, S. R.; Gullapalli, H.; Dubey, M.; Ajayan, P. M. *ACS Nano* **2010**, *4*, 6337.
(20) Qian, W.; Cui, X.; Hao, R.; Hou, Y.; Zhang, Z. *ACS Appl. Mater. Interfaces* **2011**, *3*, 2259.
(21) Li, X.; Wang, H.; Robinson, J. T.; Sanchez, H.; Diankov, G.; Dai, H. *J. Am. Chem. Soc.* **2009**, *131*, 15939.
(22) Zhang, C.; Fu, L.; Liu, N.; Liu, M.; Wang, Y.; Liu, Z. *Adv. Mater.* **2011**, *23*, 1020.

(23) Khaderbad, M. A.; Tjoa, V.; Rao, M.; Phandripande, R.; Madhu, S.; Wei, J.; Ravikanth, M.; Mathews, N.; Mhaisalkar, S. G.; Rao, V. R. *ACS Appl. Mater. Interfaces* **2012**, *4*, 1434.

(24) Long, D.; Li, W.; Ling, L.; Miyawaki, J.; Mochida, I.; Yoon, S.-H. *Langmuir* **2010**, *26*, 16096.

(25) Chen, P.; Yang, J.-J.; Li, S.-S.; Wang, Z.; Xiao, T.-Y.; Qian, Y.-H.; Yu, S.-H. *Nano Energy* **2013**, *2*, 249.

(26) Wu, J.; Zhang, D.; Wang, Y.; Hou, B. *J. Power Sources* **2013**, *227*, 185.

(27) Zheng, B.; Wang, J.; Wang, F.-B.; Xia, X.-H. *Electrochem. Commun.* **2013**, *28*, 24.

(28) Zhang, Y.; Fugane, K.; Mori, T.; Niu, L.; Ye, J. *J. Mater. Chem.* **2012**, *22*, 6575.

(29) Huan, T. N.; Van Khai, T.; Kang, Y.; Shim, K. B.; Chung, H. *J. Mater. Chem.* **2012**, *22*, 14756.

(30) Wang, P.-C.; Liao, Y.-C.; Lai, Y.-L.; Lin, Y.-C.; Su, C.-Y.; Tsai, C.-H.; Hsu, Y.-J. *Mater. Chem. Phys.* **2012**, *134*, 325.

(31) Wang, P.-C.; Liao, Y.-C.; Lai, Y.-L.; Lin, Y.-C.; Su, C.-Y.; Tsai, C.-H.; Hsu, Y.-J. *Carbon* **2012**, *50*, 1650.

(32) Zhang, L.-S.; Liang, X.-Q.; Song, W.-G.; Wu, Z.-Y. *Phys. Chem. Chem. Phys.* **2010**, *12*, 12055.

(33) Panchakarla, L.; Subrahmanyam, K.; Saha, S.; Govindaraj, A.; Krishnamurthy, H.; Waghmare, U.; Rao, C. *Adv. Mater.* **2009**, *21*, 4726.

(34) Moon, I. K.; Lee, J.; Ruoff, R. S.; Lee, H. *Nat. Commun.* **2010**, *1*, 73.

(35) Gao, W.; Alemany, L. B.; Ci, L.; Ajayan, P. M. *Nat. Chem.* **2009**, *1*, 403.

(36) Zhou, Y.; Bao, Q.; Tang, L. A. L.; Zhong, Y.; Loh, K. P. *Chem. Mater.* **2009**, *21*, 2950.

(37) Liao, K.-H.; Mittal, A.; Bose, S.; Leighton, C.; Mkhoyan, K. A.; Macosko, C. W. *ACS Nano* **2011**, *5*, 1253.

(38) Long, D.; Hong, J.-Y.; Li, W.; Miyawaki, J.; Ling, L.; Mochida, I.; Yoon, S.-H.; Jang, J. *ACS Nano* **2011**, *5*, 6254.

(39) Boukhvalov, D. W.; Katsnelson, M. I. *J. Am. Chem. Soc.* **2008**, *130*, 10697.

(40) Kim, T.; Lee, H.; Kim, J.; Suh, K. S. *ACS Nano* **2010**, *4*, 1612.

(41) Perera, S. D.; Mariano, R. G.; Vu, K.; Nour, N.; Seitz, O.; Chabal, Y.; Balkus, K. J., Jr *ACS Catal.* **2012**, *2*, 949.

(42) Kaminska, I.; Das, M. R.; Coffinier, Y.; Niedziolka-Jonsson, J.; Sobczak, J.; Woisel, P.; Lyskawa, J.; Opallo, M.; Boukherroub, R.; Szunerits, S. *ACS Appl. Mater. Interfaces* **2012**, *4*, 1016.

(43) Zhang, J.; Zhao, X. *J. Phys. Chem. C* **2012**, *116*, 5420.

(44) Ferrari, A.; Robertson, J. *Phys. Rev. B* **2000**, *61*, 14095.

(45) Nowicki, P.; Pietrzak, R.; Wachowska, H. *Energy Fuels* **2010**, *24*, 1197.

(46) Kira, A.; Matsubara, Y.; Iijima, H.; Umeyama, T.; Matano, Y.; Ito, S.; Niemi, M.; Tkachenko, N. V.; Lemmetyinen, H.; Imahori, H. *J. Phys. Chem. C* **2010**, *114*, 11293.

(47) Lahaye, J.; Nanse, G.; Bagreev, A.; Strelko, V. *Carbon* **1999**, *37*, 585.

(48) Nanse, G.; Papirer, E.; Fioux, P.; Moguet, F.; Tressaud, A. *Carbon* **1997**, *35*, 175.

(49) Reina, A.; Jia, X.; Ho, J.; Nezich, D.; Son, H.; Bulovic, V.; Dresselhaus, M. S.; Kong, J. *Nano Lett.* **2009**, *9*, 30.

(50) Ferrari, A.; Meyer, J.; Scardaci, V.; Casiraghi, C.; Lazzeri, M.; Mauri, F.; Piscanec, S.; Jiang, D.; Novoselov, K.; Roth, S. *Phys. Rev. Lett.* **2006**, *97*, 187401.

(51) Dua, V.; Surwade, S. P.; Ammu, S.; Agnihotra, S. R.; Jain, S.; Roberts, K. E.; Park, S.; Ruoff, R. S.; Manohar, S. K. *Angew. Chem., Int. Ed.* **2010**, *49*, 2154.

(52) Englert, J. M.; Dotzer, C.; Yang, G.; Schmid, M.; Papp, C.; Gottfried, J. M.; Steinrück, H.-P.; Spiecker, E.; Hauke, F.; Hirsch, A. *Nat. Chem.* **2011**, *3*, 279.

(53) Zhang, B.; Chen, Y.; Zhuang, X.; Liu, G.; Yu, B.; Kang, E.-T.; Zhu, J.; Li, Y. *J. Polym. Sci., Part A: Polym. Chem.* **2010**, *48*, 2642.

(54) Li, X.; Wang, X.; Zhang, L.; Lee, S.; Dai, H. *Science* **2008**, *319*, 1229.

(55) Wang, X.; Ouyang, Y.; Li, X.; Wang, H.; Guo, J.; Dai, H. *Phys. Rev. Lett.* **2008**, *100*, 206803.

(56) Coropceanu, V.; Cornil, J.; da Silva Filho, D. A.; Olivier, Y.; Silbey, R.; Brédas, J.-L. *Chem. Rev.* **2007**, *107*, 926.

(57) Hummers, W. S., Jr; Offeman, R. E. *J. Am. Chem. Soc.* **1958**, *80*, 1339.